Three-dimensional Analysis of Dissipated Energy in Fatigue Crack Growth

C. M. Davis and J. S. Daily

Department of Mechanical Engineering, University of Tulsa, 800 South Tucker Drive, Tulsa, OK 74104, USA; Fax: 00 1 918 631 2397; E-mail: jeremy-daily@utulsa.edu

ABSTRACT. *A recently published theory of fatigue crack growth in ductile solids proposes a relationship between the fatigue crack growth rate and the total plastic energy dissipated in the reversed plastic zone ahead of the crack. The fatigue crack growth rate estimation has been investigated for a stationary crack in mode I and has been shown to reasonably agree with ΔK^4-Paris-regime crack growth data for ductile metals. Further studies have computed the plastic dissipation in mixed mode I/II and the current study extends the calculation of plastic dissipation to include mode III loading via three-dimensional finite element analysis. A meshing scheme is presented that can resolve the reversed plastic zones in a three-dimensional specimen. The contribution to the total plastic dissipation from shear loading is shown to be larger than the numerical results for mode I.*

INTRODUCTION

Energy based fatigue crack growth rate estimations show promise in understanding and quantifying fatigue crack growth. Following other energy based approaches (e.g. [1]), Klingbeil [2] proposed a relationship between the mode I fatigue crack growth rate and the total plastic dissipation in the reversed plastic zone ahead of the crack tip. A similar approach using plastic dissipation was presented by Pandey and Chand [3]. The results of these studies suggested that an energy-based approach could estimate the Paris Law fatigue crack growth based on monotonic fracture toughness data, elastic-plastic properties, and the plastic dissipation as calculated using the finite element method. The ramification of this conclusion is that only monotonic testing would be needed for a screening of materials that will be subjected to cyclic loading in service. In other words, the fatigue crack growth rate could be estimated for a new material if only the monotonic properties were measured. This would have the potential to save time and money during the material selection process of design. However, final selection of a material will require significant relevant testing before being used in service, especially for mission critical components.

Understanding the fatigue crack growth rate has renewed importance based on the need to estimate the *minimum* life of components. Recent analysis by Jha et al. [4] suggests that the minimum number of cycles to failure is dominated by crack growth. Thus, quantifying

the number of cycles for crack initiation may not be as important if the majority of minimum service life is spent in crack growth. This study is a refinement of the damage tolerant concept used for mission critical components and provides further motivation to explore crack growth mechanisms.

Since the estimation of the fatigue crack growth rate based on plastic dissipation in mode I showed promise, the computation of the results for the total plastic dissipation energy ahead of the crack tip are interesting results in themselves. Therefore, Daily and Klingbeil [5, 6] extended the plastic dissipation calculations to mixed mode I/II using 2-D plane strain finite element analysis. These results showed that the plastic dissipation in mode II was nearly an order of magnitude higher than in mode I. Further 2-D studies examined the plastic dissipation for an interface crack between materials that had the same elastic properties but different plastic properties [7]. The numerical results for the plastic dissipation with different plastic properties (i.e. different yield stresses) were the same for a layered material when the yield stress ratio was 5/3 or higher. In other words, the contribution to the total plastic dissipation contribution comes predominantly from the material with the lower yield stress.

Other researchers have used energy-based concepts to understand and explore fatigue crack growth rates including Ranganathan et al. [8] and Cojocaru & Karlsson [9]. However, no results were found in the literature regarding the contribution to the total plastic dissipation for out-of-plane (mode III) loading. Loading contributions in mode III can occur in a variety of systems including functionally graded materials [10], gears [11], interfaces [12], out-of-plane loading [13], and in small crack growth [14]. However, other research suggests that remote mode III loading may not produce local mode III crack growth [15], which leaves the topic of crack growth with mode III components open for exploration. This paper extends the previous work to include quantification of the cyclic plastic dissipation to remote out-of-plane loading conditions. It should be noted that a rigorous experimental verification of Klingbeil's dissipated energy hypothesis for mixed mode has not been conducted for mixed mode loading and the results presented herein are computational and need experimental verification.

Overview of Plastic Dissipation

The foundation of the plastic dissipation hypothesis is that the same amount of energy is released during cyclic loading as would be released during monotonic loading of a crack propagating the same amount. The result of the argument presented in Ref. [2] states that the fatigue crack growth rate is proportional to the plastic energy dissipated in the reverse plastic zone, and that the proportionality constant is the inverse of the monotonic strain energy release rate. This expression is written as

$$\frac{da}{dN} = \frac{1}{G_C}\frac{dW}{dN} \tag{1}$$

where $\frac{da}{dN}$ is the fatigue crack growth rate, $\frac{dW}{dN}$ is the plastic dissipation, and G_C is the critical strain energy release rate. The determination of the right hand side of Eq. 1 only requires monotonic properties. This means the fatigue crack growth rate may be estimated using only monotonic test data. The plastic dissipation is defined with the integral

$$\frac{dW}{dN} = \iiint \left\{ \oint \sigma_{ij} d\varepsilon_{ij}^{p} \right\} dV. \tag{2}$$

The next section describes the process for computing the integral stated in Eq. 2 using the finite element method for all three modes of remote loading. A three dimensional model is required to capture the out-of-plane loading conditions. Once results were obtained, they were cast in a non-dimensional form and presented. In the results section, the mode III plastic dissipation results are compared to previously published mixed-mode I/II results. A discussion and conclusion section follow.

NUMERICAL MODELING PROCEDURES

Model Geometry and Material Properties

The geometry for this numerical study is based on an end notched flexure (ENF) specimen and is shown in Fig. 1. The dimensions used in all of the analyses were L=203 mm (8 in), w=50.8 mm (2 in), h=50.8 mm (2 in), and a=101.6 mm (4 in). The left face was fixed while self-equilibrating tractions were applied to the split right face.

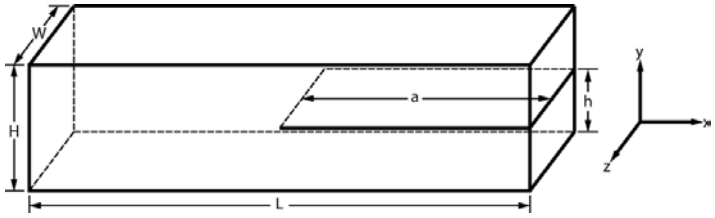

Figure 1. Model geometry.

The specimen is modelled as an isotropic, homogenous, ductile material that exhibits bilinear kinematic hardening as explained in [2, 5]. The kinematic hardening model enables plastic shakedown after one loading cycle. For this study, typical elastic values for steel were used (E=209 GPa (30 Msi), ν=0.3, σ_{yield}=248 MPa (36 Ksi), E_T/E=0.05).

Finite Element Modelling

Resolving the reversed plastic zone requires an especially fine mesh near the crack tip. In Ref. [2] the two-dimensional reversed plastic zone was resolved using crack tip elements that were 0.002% as long as the elements near the boundary. In two dimensions, crack tip

biasing schemes are available in most commercial meshing codes. Biasing a mesh towards a crack *line* in three dimensions proved difficult for general purpose meshing algorithms built into the Abaqus finite element program. Several specialty programs, such as Zencrack, FRANC3D, and FRAC3D, are tailored for meshing three-dimensional crack geometries, which can then be exported to finite element solvers. These programs can be used to mesh a wide range of crack geometries but are limited in their ability to generate a crack mesh that can maintain element quality with a high element density at the crack front. The three-dimensional meshing schemes used in the analyses by Pipkins and Atluri [16], Citarella and Crici [17], and Jin and Dodds [18] demonstrate structured meshes that successfully bias in all three dimensions. A similar approach is taken in this study.

A longitudinal cross-section cut out of the meshed geometry is shown in Fig. 2a. Along a small radius about the crack, a two-dimensional biasing scheme is simply revolved about the crack front to achieve a mesh that maintains an acceptable aspect-ratio (no long or distorted elements) and an efficiently biased crack front.

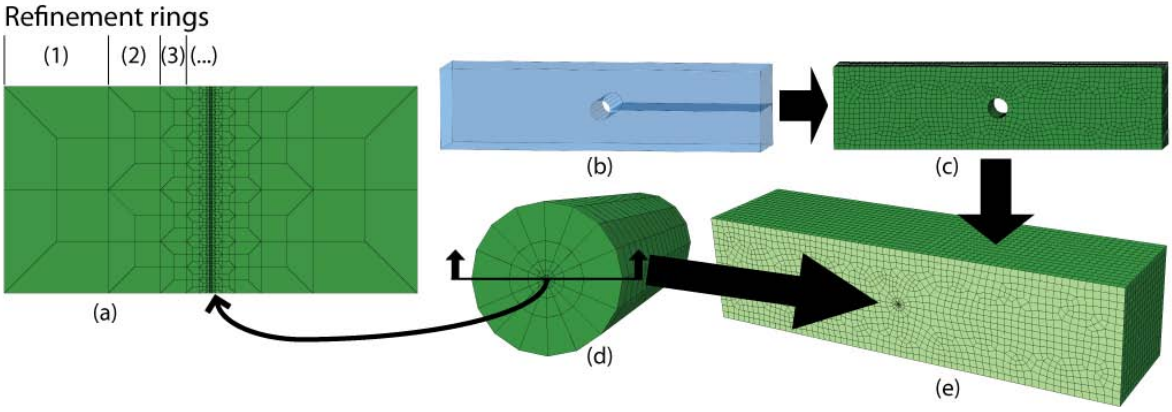

Figure 2. (a) Cross-section of crack-front mesh showing refinement rings (b) Unmeshed geometry with void for crack front elements. (c) Abaqus-meshed geometry with void. (d) Script-generated crack front elements. (e) Assembled mesh.

The geometry under consideration was meshed in a multistage process. The first step used a custom Python script to define the elements and nodes in a prismatic volume surrounding the crack front (Fig. 2d). The second step used the automatic meshing routines in Abaqus to generate the mesh for the global geometry (Fig. 2c). Finally, these two meshes were merged to yield the fully meshed specimen (Fig. 2e). The elements used were 20 noded hexahedral elements with reduced integration (C3D20R in the Abaqus element library).

It is important to point out that the finite element solution is applicable to continuum modelling of the solid. The numerical results are solutions to the response of the material for small-scale elasto-plasticity with a von Mises yield criterion. Application of these

results to material systems that violate the continuous media assumption may be inappropriate.

To ensure convergence of the numerical solution, three meshes were generated employing successively higher numbers of elements around the crack front and the plastic dissipation from each of these meshes was compared. The number of elements was controlled by changing the number of refinement rings around the crack front (each additional ring uses elements half the size of the elements in the previous ring).

Loads and Boundary Conditions

The loading conditions used in this study were applied to the right hand faces of the geometry in Fig. 1 using a generalized traction vector (TRVEC in Abaqus). The goal was to load the specimens in a similar manner as those shown in many introductory texts on fracture mechanics when describing the modes of loading. A fixed boundary condition was applied on the left side of the geometry. Since the loads for mode I are self-equilibrating, the boundary conditions simply prevent rigid body modes. For modes II and III, the fixed boundary provides a reaction to the torque applied by the shear loading.

The magnitudes of the loading applied in this study were chosen to maintain small scale yielding while still maintaining a reversed plastic zone that can be efficiently resolved using the aforementioned meshing scheme. The magnitude of the applied tractions was 5.516 MPa (800 psi) for mode I, 124.1 MPa (18,000 psi) for mode II and 5.516 MPa (800 psi) for mode III. These loads translate to the linear elastic fracture mechanics parameters shown in Table 2 on the following page.

The stress intensity factors (SIFs) and J-integral were determined using the *CONTOUR INTEGRAL keyword in Abaqus on a 3-D elastic only analysis. A total of 5 contours were specified and the average of the results through the thickness are reported in Table 2. As expected, the SIFs and J-integral had higher magnitudes near the surface with minimums in the center. Of note was the mode II component in the mode III loading case. While the table reports an average of near zero, the magnitudes of KII were nearly linearly distributed across the thickness with a maximum value of over 10 MPa√m. This result is expected because the effect of the remote tearing action produces a mode II load at the crack front near the edges.

Table 1. Linear elastic fracture mechanics parameters for different global loading conditions as calculated using the contour integral in Abaqus.

Remote Loading	KI (MPa√m)	KII (MPa√m)	KIII (MPa√m)	J-integral (N/m)
Mode I	14.4	4.0E-4	1.8E-8	95.2
Mode II	0.58	9.89	2.6E-7	46.6
Mode III	4.02E-09	8.6E-17	4.0256	28.3

It should be noted that the strain energy release rate G can be computed from the stress intensity factors as

$$G = \frac{1-\nu^2}{E}\left({K_I}^2 + {K_{II}}^2\right) + \frac{(1+\nu)}{E}{K_{III}}^2. \quad (3)$$

Also, for linear elastic fracture mechanics, the value of $G = J$. This equality is used to verify that the small scale yielding assumption is maintained.

Plastic Dissipation

The extraction of the plastic dissipation as a quantity is trivial with the commercial software, as Abaqus maintains a history record of the desired quantity with the ALLPD variable. However, the determination of the plastic dissipation ahead of the crack tip requires four load steps to setup the cyclic reversed plastic zone ahead of the crack. The first step applies loading that develops the forward plastic zone. The second step removes the loading and creates the first reversed plastic zone. Once this initial cycle is completed, the reversed plastic zone is present and a subsequent cycle will result in a change in the total plastic dissipation as shown in Fig. 5a. The forward to reverse loading ratio for this case is R=0. The effect of the load ratio was shown to be small when estimating the mode I fatigue crack growth rate by Klingbeil [2].

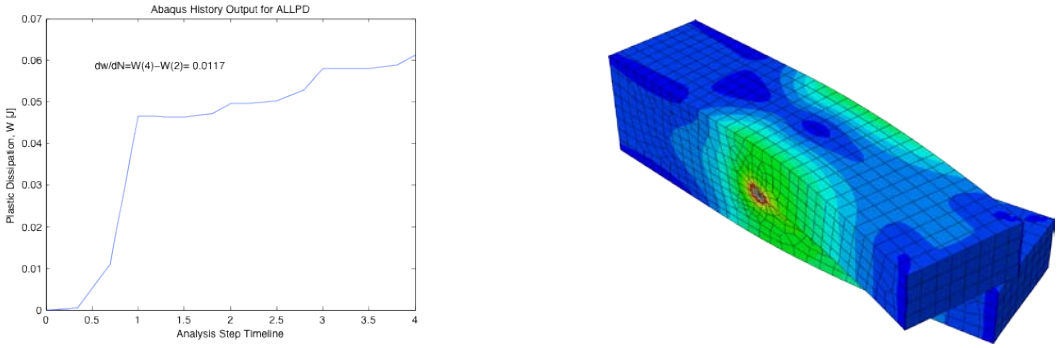

(a) (b)

Figure 5. (a) Plastic dissipation results using the ALLPD history output in the Abaqus finite element software and (b) Corresponding remote mode III loading.

RESULTS AND DISCUSSION

It is obvious that increasing the load will increase the plastic dissipation. Furthermore, the yield stress of the material affects the results. Therefore, to determine the contribution of different loading and material properties, the numerical result for the plastic dissipation should be put into a non-dimensional form according to Eq. 4.

$$\frac{dW^*}{dN} = \frac{{\sigma_y}^2}{E\Delta G^2}\frac{dW}{dN} \quad (4)$$

After inserting $\frac{dW}{dN}$ extracted from the load history data into Eq. 4, the data can be cast in a non-dimensional form as shown in Table 2. The dimensionless results for homogeneous materials depend on the hardening modulus and, to some extent, Poisson's ratio. The total plastic dissipation ahead of the crack as computed by the 3-D models is bounded by the plane stress results on the high end and plane strain results on the lower end, which is an expected result.

A convergence study was performed using the meshing algorithm previously described by increasing the number of refinement rings. The coarse mesh had 7 rings of elements and produced a total of 451,468 nodes with 116,128 elements. The medium mesh used 8 rings and had a total of 822,206 nodes and 214,432 elements. Finally, the fine mesh used 9 rings with a total of 1,563,632 nodes and 411,040 elements. The results in Table 2 show convergence of the medium mesh as the fine mesh produced around a 1% change in the final result.

Table 2. Convergence of the dimensionless plastic dissipation $\frac{dW^*}{dN}$ for different mesh designs and global loading conditions. Results are presented for $E_T/E=0.05$.

Mesh	Mode I	Mode II	Mode III
3-D Coarse	0.00586	0.0928	0.0946
3-D Medium	0.00574	0.0966	0.0990
3-D Fine	0.00568	0.0982	0.0985
2-D Plane Strain	0.00467	0.0740	N/A
2-D Plane Stress	0.0200	0.101	N/A

It is clear from the results that the shear modes of loading have a higher plastic dissipation than the mode I loading by over an order of magnitude. This suggests that a larger amount of work needs to be done on the material to propagate a crack in mixed mode, which supports the observation that a majority of cracks propagate in mode I. However, the authors suspect the mode III results to be artificially high due to the presence of mode II conditions across the crack front. This issue needs to be explored further.

In light of Eq. 1, the fatigue crack growth rate has the potential to be estimated if the critical strain energy release rate (i.e. fracture toughness) is known. However, the fracture toughness is mode dependent and data is limited for mode II and III toughness. Interesting applications for mixed mode I/II/III fatigue crack growth arise from interfaces of different materials where sustained debonding can exist.

CONCLUSION

The plastic dissipation in the reversed plastic zone ahead of a stationary crack was determined using the finite element method. All three modes of loading were explored by varying the traction vectors to a generic end notched specimen. The results were cast in a non-dimensional form and show a significant increase in the plastic dissipation when shear modes are present.

ACKNOWLEDGEMENTS

The authors would like to thank Steve Tipton for his comments and insight. This material is based upon work supported by the U.S. Air Force Research Laboratory, Propulsion Directorate (AFRL/RZTS) under Prime Contract No. FA8650-08-D-2806 Task Order 0009 and Universal Technology Corporation (UTC) Subcontract Agreement No. 09-S590- 0009-17-C4. Any opinions, findings and conclusions or recommendations expressed in this material are those of the authors and do not necessarily reflect the views of AFRL/RZTS or UTC.

REFERENCES

[1] Bodner SR, Davidson DL, Lankford JA. *Eng Fract Mech* 1983;17(2):189-191.
[2] Klingbeil N. *Int'l Journal of Fatigue* 2003;25:117-128.
[3] Pandey K, Chand S. *Int'l Journal of Fatigue* 2003;25(8):771-778.
[4] Jha SK, Caton MJ, Larsen JM. *Mat. Sci. and Engr. A* 2007;468-470(SPEC. ISS.):23-32.
[5] Daily JS, Klingbeil NW. *Int'l Journal of Fatigue* 2004;26(7):727-738.
[6] Klingbeil NW, Daily JS, Baudendistel C. *Key Engr. Materials* 2008;378-379:385-404.
[7] Daily JS, Klingbeil NW. *Int'l Journal of Fatigue* 2006; 28(12):1725–1738
[8] Ranganathan N, Chalon F, Meo S. *Int'l Journal of Fatigue* 2008;30(10-11):1921-1929.
[9] Cojocaru D, Karlsson AM. *Int'l Journal of Fatigue* 2009;31(7):1154-1162.
[10] Forth S. *Engr. Fract. Mech.* 2003;70(15):2175-2185.
[11] Spievak L, Wawrzynek P, Ingraffea A, Lewicki D. *Eng Fract Mech* 2001;68:53-76.
[12] Liu P, Cheng L, Zhang Y. *Scripta Materialia* 2001;44:487-492.
[13] Buchholz F, Chergui A, Richard H. *Eng Fract Mech* 2004;71(4-6):455-468.
[14] Yates JR, Mohammed RA. *Fatigue & Fract of Engr Mat and Struc* 1996;19(10):1285-1290.
[15] Pokluda J, Trattnig G, Martinschitz C, Pippan R. *International Journal of Fatigue* 2008;30(8):1498-1506.
[16] Pipkins DS, Atluri SN. *Finite Elements in Analysis and Design* 1996;23(2-4):133-153.
[17] Citarella R, Cricrì G. *Advances in Engineering Software* 2009;40(5):363-377.
[18] Jin ZH, Dodds RH. *Eng Fract Mech* 2004;71(12):1651-1672.